# RADInspector: Radioisotope Identification and Measurement

Aman Kataria, Johnny Klarenbeek, Dean Sullivan, David Valentine

School of Electrical Engineering and Computer Science, University of Central Florida, Orlando, Florida, 32816-2450

***Abstract*—A hand-held, high resolution $\gamma$-ray spectrometer that operates at room temperature over a wide-range of photon energies has been developed. It consists of a small volume Cadmium Zinc Telluride (CZT) compound semiconductor detector coupled to a low-noise charge preamplifier circuit. Additional analog circuitry includes 4-stages of signal conditioning for pulse shaping and gain adjustment. and a rectifier and peak/hold circuit were built for ADC (5 MSPS) preparation. An STMicro STM32F303VCT6 microcontroller was used for interfacing the analog and power peripherals (spectrometer pulse signal, battery charge level, power regulation / control, charge control) as well as the digital peripherals (USB data, SD card flash storage). The microcontroller integrates all of these peripherals and enables a robust user experience through the use of a color LCD touch screen. The spectrometer records data over a wide-range of engergies and plots it as a spectrum, saves or loads the data to / from an SD card, and transfers data to a computer via USB.**

***Index Terms* – Spectroscopy, data acquisition, low-noise preamplifier, semiconductor detectors, digital filters**

## I. Introduction

Gamma-ray spectroscopy is an important analytical tool used daily in both fundamental and applied research, and technology. However, while $\gamma$ spectroscopy has been available for decades, the field still utilizes technology such as scintillation counters or liquid cooled germanium detectors that are cumbersome to use, difficult to produce, and expensive. Reliance on these technologies is due to the necessity of achieving high resolution and efficiency for collected results. However, with the onset of improved processing techniques and availability room-temperature $\gamma$ spectrometer systems may be developed that meet both resolution and efficiency requirements.

The primary specification of the project is to produce a low-cost, portable spectrometer capable of accurately quantify $\gamma$-ray emissions from radioactive sources over a wide energy range (5keV-1MeV) through the use of a semiconductor detector. In order to achieve this, we must obtain a good signal to noise ratio, high energy resolution, and high efficiency. A small volume compound semiconductor (CZT) will be used to obtain high efficiency and good resolution. A low noise charge preamplifier will be coupled to the detector, shielded from visible light, and actively cooled by a thermoelectric cooler (TEC) in order to limit noise. In addition, the signal will be conditioned by a low noise, multi stage amplifier design. Because solid state detection of gamma radiation produces a very small amount of charge on the semiconductor, a well designed amplifier is crucial for improving SNR. The spectrometer will have a digital interface accessible through a color LCD screen with touch panel or tactile button input. Software features will include capturing and plotting gamma ray emissions on an energy histogram as well as auxiliary functions such as basic gamma dosimetry and FWHM display. The user will be able to save and load data from plots onto external data storage. The detector will be portable (battery powered) and light weight. A block diagram showing the main components of our system is shown in figure 1. A list of the major design specifications is given below:

- Low power consumption ($< 3W$)
- Long batter life (4 hr with TEC off)
- Room temperature operation
- $<$ 5 keV FWHM @ 59 keV ($^{241}Am$)
- $<$ 10 keV FWHM @ 611 keV ($^{137}Cs$)
- Plot spectrum and perform real-time dosimetry
- Low cost ($< \$500.00$)

The rest of the paper is organized as follows. First, the semiconductor detector specifications, figures-of-merit, and operation will be introduced in II. We will then present the analog circuit design specifications including the charge preamplifier, pulse-shaping circuitry, and rectifier and peak/hold circuit for ADC preparation in III. Next, the digital hardware and software components will be presented in IV and V. The power specifications, including high-voltage detector supply bias and TEC design will then be presented in VI. Finally, conclusions will be drawn in VII.

## II. Semiconductor Detector

Collisions of $\gamma$-rays within a semiconductor detector will transfer energy via the photoelectric effect, Compton scattering and pair production. For each type of interaction an electron-hole pair (EHP) is generated with energy proportional to that of the incident radiation and characteristic of the type of interaction. A photoelectron has energy directly proportional to the gamma ray and therefore has a monolithic energy distribution that is typically Gaussian in shape. A Compton EHP typically has less energy than the incident gamma ray, which is determined by an angle of recoil that spans 180°. The distribution is typically flat over a range of energies and then displays a characteristic exponential edge. Pair production will not be considered because it occurs at energies above 2 MeV,

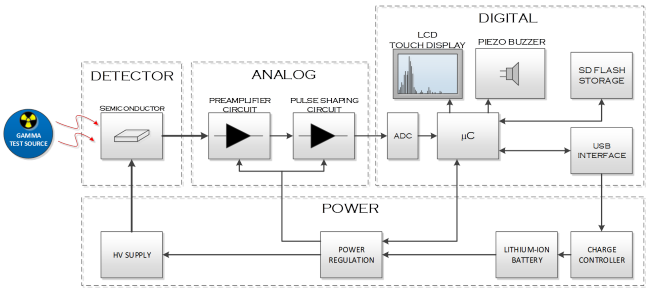


Fig. 1. Flowchart of $\gamma$ spectrometer subsystems.

which is far outside our detectors response. When energy $E_o$ is deposited due to $\gamma$ interaction it will produce $N = \frac{E_o}{\epsilon}$ mobile carriers, where $\epsilon$ is the ionization energy for the semiconductor. Under an applied bias, the mobile carriers will drift towards their corresponding oppositely charge electrodes, which generates a photocurrent. However, the deposited $\gamma$ energy is proportional to the deposited charge via $Q_{gen} = \frac{qE_{ph}}{\epsilon}$ so that the detector will be attached to a charge-sensitive preamplifier that produces an output voltage pulse proportional to the integral of the current.

In order to achieve the design goals of high resolution and efficiency, as well as good FWHM ($< 10keV$) several detector specifications must be met. A semiconductor with a large atomic number Z will result in a high stopping ability as the two quantities are proportional. This will ensure useful interaction and allow for a wide-range of $\gamma$ energies to be recorded. There must also be a high probability of photoelectric interaction in order to improve characteristic radioisotope identification by the user. The probability of photoelectric interaction is proportional to Z as $P.E. \propto Z^n$. In order to accurately record spectra, the generated charge should be linear with respect increasing $\gamma$ interaction. Both the quantum efficiency (Q.E.) and responsivity of the detector should be as close to ideal as possible (100%). All of these parameters result in a highly resolved spectra, such that it is easy to distinguish two closely spaced $\gamma$ peaks. To meet these design goals we used a CZT semiconductor detector, shown in 2, that has a $100mm^2$ active area so that the probability of interaction is high Charge generated in the bulk/surface suffers from generation-recombination trapping, decreased efficiency, and non-uniform current. Decreased activity in these regions is ideal and a thick detector (5mm) enables this to occur by increasing the likelihood that the generated charge will occur in the depletion region. Some properties of CZT are given in the table below:

The high atomic # allows for excellent stopping ability of large eV $\gamma$ particles and increases the probability of photoelectric interaction. The large bandgap decreases resolutions, but only slightly compared to the good resolution of Si (1.14 eV), so that we are sacrificing resolution for efficiency. However, the statistical noise is decreased from that of lower bandgap materials so that our SNR will improve. The Q.E. and responsivity are excellent across a wide range of energies as can be seen in figure 3, however they drop off after roughly

TABLE I
CZT PROPERTIES

| Property | CZT |
|---|---|
| Atomic Number | 49 |
| Band Gap Energy (eV) | 1.44 |
| Activation Energy (eV) | 4.8 |
| Resolution % FWHM 662 keV | 3.2 |
| $e^-/h^+$ Mobility $(cm^2/Vs)$ | 1350/120 |
| $\tau_e/\tau_p$ ($\mu$s) | 1/0.05 |
| Breakdown Voltage (V) | $< 350$ |

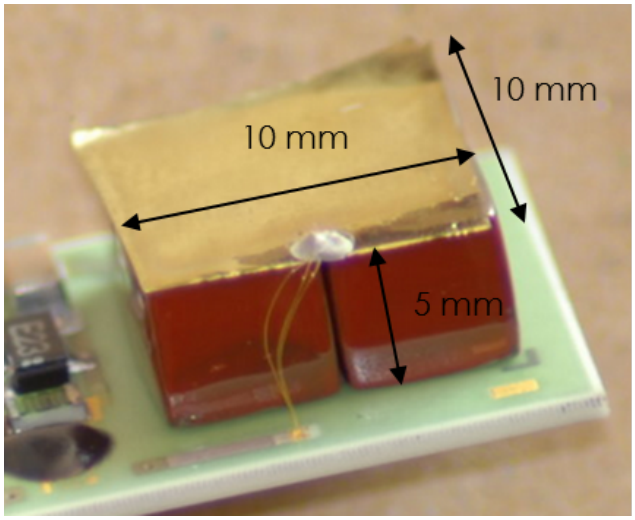


Fig. 2. Cadmium Zinc Telluride crystal ($10mmx10mmx5mm$).

100 keV. In order to account for this efficiency calibration will be performed on the spectral data whereby, for a given energy $> 100$ keV, a corresponding inverse correction will be applied to the collected counts. This will effectively re-scale the spectrum by pushing the higher energy peaks up.

The largest cause for concern is the hole mobility and risetime. The slow hole mobility causes hole tailing due to charge trapping and degrades the spectrum by decreasing FWHM. Slow risetime attenuates the pulse by increasing the rising edge of the signal and therefore adds error to the spectrum. Both can be improved by applying a high reverse voltage bias to the detector and incorporating a Frisch collar. We were only able to apply the former due to space constraints.

## III. FRONT-END ELECTRONICS

The gamma ray detector is housed in a metal probe separate from the main board in order to ensure a low noise environment and to increase measurement flexibility. The probe houses both the detector and a charge sensitive amplifier. The output of the charge amplifier is buffered by an instrumentation amplifier on the main board to help reject common mode noise that may be present on the signal. The signal is then amplifier with a fixed gain and band limited before being rectified and sampled by the microcontroller. The STM32F303VCT6

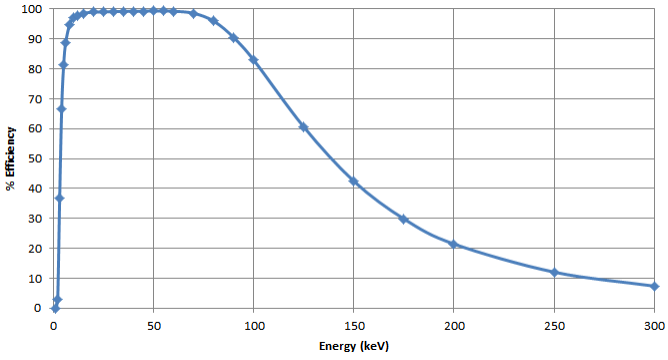


Fig. 3. CZT efficiency data for photoelectric interaction.

microcontroller was chosen in part due to its high speed analog to digital converter (5 MSPS).

### A. Charge Amplifier

Figure 4 shows the detecter connected to the charge amplifier. To reduce the size of the schematic power supply filtering components have been omitted. The detector is biased to 500V and current limited with a 100M resistor. Complete noise analysis was performed on the charge amplifier to optimize component selection in order to maximize the output signal to noise ratio (SNR). Charge produced by gamma rays in our measurement range is typically on the order of a few femto Coulombs (fC), which will result in an output pulse of a few hundred uV to several mV with a charge amplifier feedback capacitance of 1pF. This poses a serious problem when typical noise contributions of the op amp, resistors, and detector are considered. In order to optimize the choice of components with respect to noise, the contribution of the op amps voltage and current noise, the detectors current noise, and the feedback resistors thermal noise were fully modelled 6. The output contribution of each of these noise sources can be represented by the following equations:

$$V_o = (I_{nrsh} + I_{nD} + I_{nOPA})\frac{A_o R_{sh} R_f}{D(s)} \tag{1}$$

$$V_o = E_{nOPA}\frac{A_o(s)[(C_o + C_f)R_{sh}R_f(s)R_{sh} + R_f]}{D(s)} \tag{2}$$

$$V_o = E_{nRF}\frac{A_o(s)R_{sh}}{D(s)} \tag{3}$$

$$A_o(s) = \frac{A_o(DC)}{1 + s/\omega_o}, \omega_o = \frac{\omega_{GBWP}}{\sqrt{2}A_o(DC)} \tag{4}$$

$$D(s) = C_f(A_o(s) + \frac{C_D}{C_f} + 1)R_{sh}R_f s + A_o(s)R_{sh} + R_{sh} + R_f \tag{5}$$

Variables starting with $I_n$ are current noise densities and those starting with $E_n$ are voltage noise densities. Op amp voltage noise density was fully modelled including 1/f and flat band noise as specified in op amp datasheets. Temperature dependence of the detectors shot noise due to leakage (dark) current was also modelled. Noting that the majority of the noise contribution was due to current noise (both from detector and op amp), an N-channel JFET (NXP BF862) was used to buffer the op amps inverting input. Since the JFETs high current gain effectively isolates the op amps inverting input from the feedback loop, and because the JFET bias resistor is much smaller than the feedback resistor, we can essentially ignore the op amps current noise contribution and simplify the analysis.

Shown in Fig. 3 is the output referred voltage noise densities due to current noise (in red), thermal noise from the feedback resistor (green), and the op amps voltage noise (blue). Several observations were made from the transfer functions of the noise sources. Current noise from the detector due to leakage current dominates. While physical characteristics of the detector that influence leakage current cannot be altered, the detectors operating temperature can be reduced. This

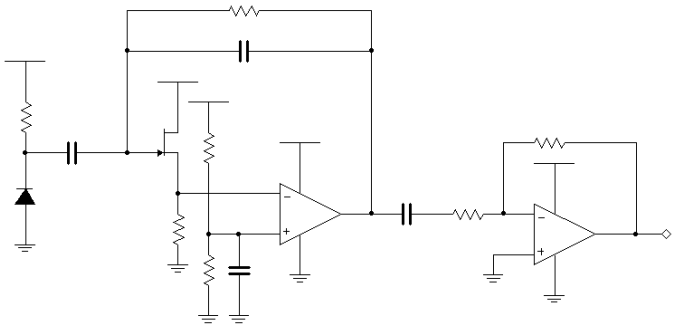

Fig. 4. Charge amplifier circuit with output buffer.

can have a large impact on detector current noise. Cooling down the feedback resistor will also reduce its thermal noise contribution. Finally, reducing the detector capacitance and increasing the feedback capacitance will reduce the peak in the op amps voltage noise density.

Since the amplifiers charge gain is dependent on the feedback capacitance in the circuit, its value cannot be increased to reduce output referred noise. Instead we optimized the op amp by computing the total output referred voltage noise for a variety of low noise op amps. This process was automated to compute RMS output noise voltage at room temperature and at -70C. The analysis was performed assuming a detector with capacitance of 15pF, detector shunt resistance 5G a feedback resistor of 100M, a feedback capacitor of 1pF, and detector leakage current of 5nA. The results are displayed in II.

The AD8622 op amp was chosen for the charge amplifier to accommodate the 5V single supply design and because it

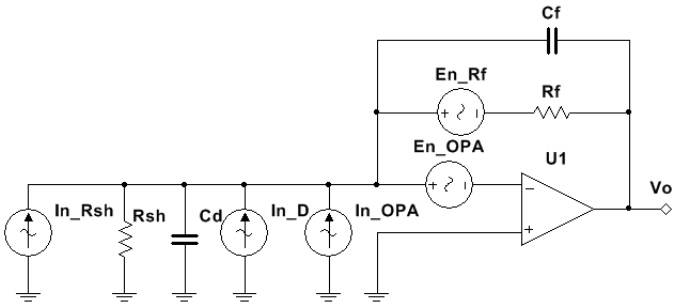


Fig. 5. Noise sources modelled for charge amplifier noise analysis.

TABLE II
NOISE ANALYSIS RESULTS FOR OPAMPS

| Opamp | RMS(mV)@298K | RMS(mV)@230K |
|---|---|---|
| OPA1612 | 2.63 | 0.46 |
| OPA827 | 2.66 | 0.46 |
| OPA2209 | 2.62 | 0.47 |
| AD8622 | 2.40 | 0.47 |
| LMP7721 | 2.78 | 0.47 |
| LT1028 | 2.54 | 0.85 |
| AD8397 | 3.10 | 0.96 |
| OPA211 | 2.59 | 0.97 |
| LME49990 | 2.61 | 0.97 |

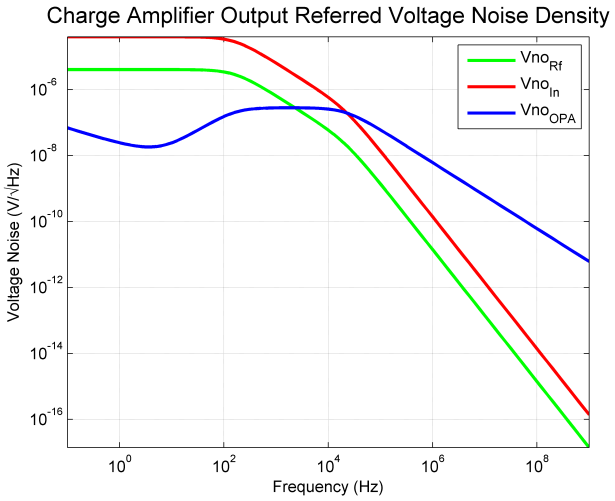


Fig. 6. MATLAB simulation of output referred voltage noise densities due to circuit noise sources.

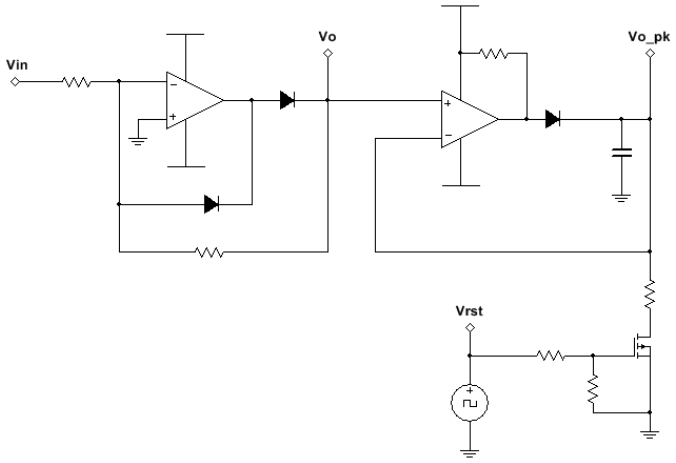


Fig. 7. Precision rectifier and peak hold/reset circuit.

will provide the best SNR at room temperature. The JFET is biased at 1mA drain current with V+ = V- = 2.5V. A 1pF feedback capacitor and 100M feedback resistor was chosen in the final design to maximize charge to voltage gain and input impedance.

### B. Signal Conditioning

A gain of 50-100 is applied to the charge amplifier output to scale it to a measurement range of either 0-400keV or 0-1MeV. This is accomplished using several reconfigurable stages in a quad op amp. The signal is also conditioned for the analog to digital converter by limiting the bandwidth to 2MHz in each gain stage. This is done to ensure that we meet the Nyquist sampling criterion. This amplifier stage is powered by a bipolar supply of 5V. Before the pulse signal is sampled it is rectified and scaled to the microcontrollers analog reference voltage (3.3V). A simple high speed half wave precision rectifier circuit was designed for this purpose. This was necessary because while the ideal charge amplifier response for a charge impulse is a single sided exponential decay, the pulse signal will contain some overshoot which will momentarily saturate a single supply amplifier. A negative input to the ADC could also damage it. The rectified signal output is connected to the microcontrollers ADC and to a peak hold circuit using a comparator which will track the peak value of the pulse until the capacitor is reset using an N-channel MOSFET. This peak value is also sampled by the ADC. This analog peak detect implementation was chosen in order to retain some flexibility in the signal processing path. The peak value can be sampled from the circuits output and it can be measured from the pulse signal input, or both can be measured and averaged to reduce noise. Figure 7 shows the precision rectifier and peak hold circuitry. The $V_o$ and $V_{opk}$ signals are scaled and buffered by a dual op amp before they are sampled by the microcontroller. This ensures that the signal has a low enough impedance to drive the analog to digital converter at all frequencies. The $V_{rst}$ connection is driven by one of the GPIO pins on the microcontroller and can be used to reset the peak hold circuit by turning on the MOSFET to discharge the output capacitor.

### C. Signal Sampling

Sampling of gamma ray pulses is completely interrupt driven on the microcontroller in order to maximize code efficiency. The analog to digital converter is configured to continuously write to a ring buffer using a direct memory access (DMA) controller. A comparator peripheral is also configured to read ADC values and triggers an interrupt when the sampled pulse value exceeds a software programmable threshold on a rising edge of the signal. A timer is then triggered to ensure that the full pulse is sampled and stored in the ring buffer. The timer then triggers an interrupt which configures the DMA controller to initiate a transfer of the sampled pulse from the ring buffer to a dedicated buffer for processing. Upon completion of the DMA transfer a flag will be set which is checked in the main program loop to notify the MCU that a pulse has been sampled and is ready to be processed. This implementation avoids wasting time polling the ADC and checking each arriving sample for a rising edge crossing. This is important in our device as this time needs to be allocated to process pulses and take care of user interface, updating the screen, and transferring data over SPI / SD card / USB.

## IV. Digital Hardware

The digital hardware design of this project focused on interfacing the analog and power peripherals (spectrometer pulse signal, battery charge level, power regulation / control, charge control, etc) as well as digital peripherals (USB data, SD card flash storage) to a microcontroller. The microcontroller integrates all of these peripherals and enables a robust user experience through the use of a color LCD touch screen. The spectrometer records data and plots it on a gamma spectrum, saves or loads the data to / from an SD card, and transfers data to a computer via USB.

### A. Microcontroller

In order to implement these features it is important to utilize a fast microcontroller with many digital and analog peripherals and a sound architecture such as the 32-bit ARM architecture. Also, a fast microcontroller was needed for fast signal processing. We used the ARM Cortex M4 based STMicro STM32F303VCT6, some of the most noted features are below:

- High speed (72MHz), large flash (256K), and large RAM (48K)
- Integrated hardware floating point unit (FPU)
- High speed ADC peripheral (up to 5MSPS)
- Large number of GPIO pins (87, 42 of these 5V tolerant)
- UART, SPI, I2C, USB peripherals

### B. Touchscreen

An important aspect of the gamma spectrometer is a professional and user friendly interface provided through a color LCD screen capable of displaying fairly high resolution gamma spectrum plots and other useful data. The SainSmart LCD touchscreen was used; it is 3.2, 320 x 240 RGB, has a PCB adapter and SD slot. It uses the TI ADS7843 touch screen controller, which is a popular 12-bit analog to digital converter used to drive 4 wire resistive touch screens. The part has a SPI interface, the SD card was interfaced to the microcontroller through SPI. The touch screen controller and SD card slot has a pinout for chip select lines, meaning the SPI control lines are conveniently tied to the same peripheral interface on the microcontroller. The board features a popular LCD controller, SSD1289, has a 20 bit parallel interface comprising 16 data lines and 4 control lines. device.

## V. Software

When designing a project which involves the use of many different peripherals it is essential to organize and distribute the code between different classes. Each peripheral and set of device functions has their own class of functions and data structures, linked and accessed by the main program loop. Some of the main features are discussed.

### A. Graphical User Interface

The user friendly interface required using the SSD1289 controller to communicate with the microcontroller and the LCD screen. The class TouchLogic.c and SSD1289.c are both needed to have a GUI. It contains both low level and code necessary to communicate with the SSD1289 LCD controller as well as the high level graphics functions needed for drawing the devices GUI. Several high level functions were used to for drawing lines, filled and unfilled boxes. The menu at the top left of the screen enables the user to save a file or open a new one if stored in devices flash. When the spectrum is plotted the user can also select an energy peak via user input on the touch screen to identify its FWHM and energy amplitude value in kEV of each peak.

Figure 8 shows the touchscreen interface where the spectrum is displayed. On the top left we have File, the user is prompted with the options of New and Open, these options allow the user to create a new file or to open an existing file that is stored in flash. In Settings the user has the option to turn the audio feedback on/off, enable discriminator threshold mode, perform efficiency calibration, and add a pulse waveform overlay on the histogram. The current screen is displaying a recorded spectrum. The user can select a peak on the histogram and it will display the peak (pk), full-width-half-max ("FWHM") on the top right of the screen in a box. The scale is currently set at 0 to 400 kEV. In the top right corner, the battery meter is displayed for the users benefit. Not shown is the real-time dosimeter that displays both counts-per-second and total counts next to the battery meter. These features enhance the user interface and make the device more user friendly.

### B. Drivers

There are several drivers needed to have functioning peripherals. The ADS7843 is a 12- bit successive approximation ADC with a synchronous serial interface and low on resistance switches for driving touch screens, the file ADS7843drv.c enables communication with the touchscreen via SPI interface. Some other important drivers are, drivers written for the SD card and USB; SD.c and USB.c, which allow the user to save data on SD card or load data to PC via USB.

### C. Signal Processing

The output signals from the preamplifier are directly digitized and then filtered and optimized using digital signal processing techniques. Digital signal processing techniques provide a higher degree of freedom, better stability and better resolution over analog. Figure 9 shows the original signal for Barium 133. We implemented a 12th order FIR filter low pass filter in MATLAB. The low pass filter is used to filter out statistical fluctuations, but also filter out some of the high frequency signals that cause distortion of the signal. Figure 9 shows the low pass filter is smoothing the original signal. After implementing this technique we saw significant smoothing in

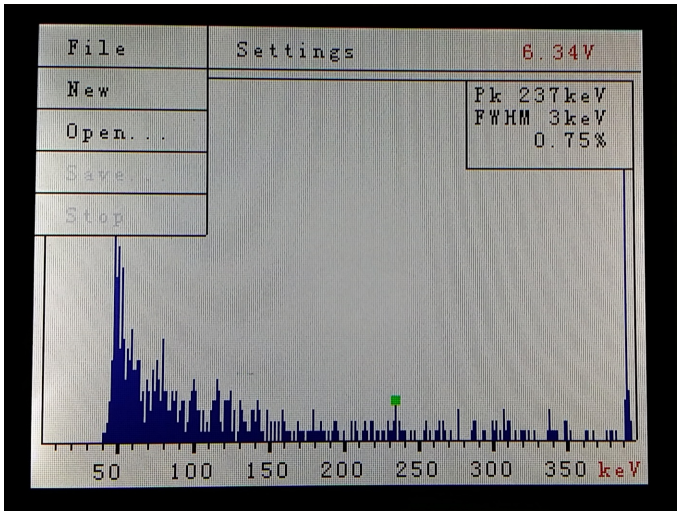


Fig. 8. Example spectrum and several features of RADInspector.

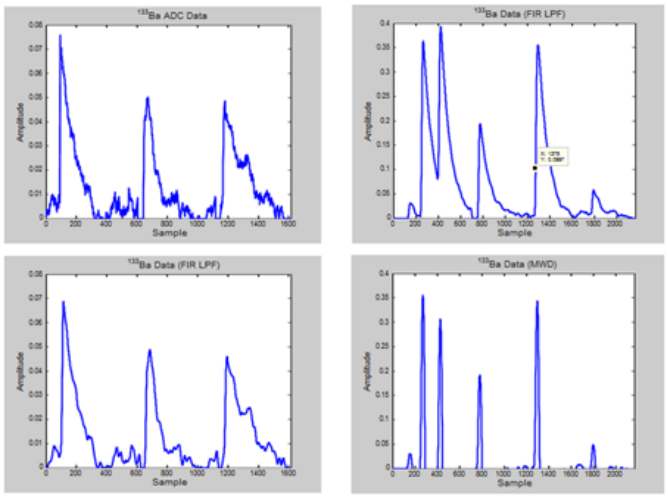


Fig. 9. *left* Original Ba-133 sampled data (*top*) and Ba-133 sampled data after applying LPF (*bottom*) *right* Ba-133 data after applying an FIR low-pass filter (*top*) and Ba-133 data after applying MWD (*bottom*).

the signal, however, we needed to further enhance the signal to extract useable data. Moving window deconvolution (MWD) algorithm was implemented after the LPF, to further enhance the signal. This algorithm deconvolves unwanted convolution, it compensates for undesired convolution which causes additional noise and inaccurate measurements. Moreover, a gamma ray is an impulse, while the output of the detector resembles a single sided exponential which is the impulse response of the system. The information that is extracted from the output signal is the amplitude of each pulse, which is proportional to the energy of the gamma ray that generated it. In order to identify isotopes, the peaks of interest for each isotope needs to be identified, which is the amplitude of each pulse. MWD also assists in pile up rejection, when pulses are coming in at a high count rate they overlap which causes inaccuracies in energy amplitude measurements. Figure 9 shows the extracted energy amplitudes and no overlap of the signals, improved count rate and smooth peaks. As shown in the following figures, the energy amplitudes were successfully recovered after implementing this signal processing techniques.

## VI. Power

The RadInpsector utilizes low noise power regulators and multiple decoupling elements to reduce noise and any unwanted disturbances to pulsed signals entering the ADC of the STM microcontroller. The maximum power consumed by the system is approximately 1.5 watts with a current draw of 300 mA and voltage operations at +5, -5, and 3.3 volts. Depicted below in figure 10 is a block diagram indicating the chosen components used in regulated power throughout the devices subsystems.

The device is powered by two 18650 lithium-ion batteries that are configured in series to establish a maximum supply voltage of 8.4 volts. The 8.4 volts allows for a sufficient amount of voltage to be regulated down linearly so as to avoid switching element usage. The batteries will be charged through USB communication protocols between the host PC and the STM microcontroller. The charge current is limited to 500 mA by both the USB protocol and the LT1513 charge controller, which in turn allows for a depleted 18650 battery to become fully charged within 4.6 hours. The LT1513 charge controller was chosen due its intended design of charging lithium batteries through their proper constant-current/constant-voltage (CC/CV) cycles and having high charging current for USB charging applications.

The STM microcontroller is power regulated via a 3.3 volt LT1962 voltage regulator, chosen specifically to allow a maximum current draw of 300 mA so as to satisfy the I/Os and digital peripherals that are both currently used and may be used in future enhancements. Though the IC regulator is rated for 300 mA, only 40-50 mA is consumed by the microcontroller and peripherals with the features that are currently implemented. The peripherals powered include the LCD controller, LCD backlight, and SD card. The power regulated to the microcontroller will always be active while the spectrometer is switched on, and regulation to the other components will only be active once the shutdowns pins on the regulators are set high by the microcontroller. This added feature was for the purpose of troubleshooting for the user, if needed to save on power consumption.

The LTC1174 regulator is used to invert the battery voltage and buck regulate it down to negative (-) 5 volts. The negative five volt supply is required so that the pulse processing amplifiers can not only operate properly, but allow for capturing of any pulses on the negative swing. The MAX5091 linear 5 volt regulator is utilized for its wide input range and low microvolt noise characteristics. Also, the MAX5091 regulator supports 50 millvolts of maximum dropout voltage, which is ideal in battery powered devices that operate linearly at low voltages. The positive (+) 5 volt supplies the preamplifier, pulse shaping amplifiers, magnetic buzzer, and bias circuitry. The analog circuitry consumes approximately 30-40 mA and the bias circuitry up to 50 mA, resulting to less than half a watt of power consumption.

The LT1930 boost converter IC is used to supply high voltage to the CZT crystals so that junction capacitance can be decreased and charge transfer is improved. The high voltage module is capable of delivering 90 volts when the input voltage pin set to (+) 5 volts. The voltage input to the module comes from the the positive 5 volt regulator stated previously, the

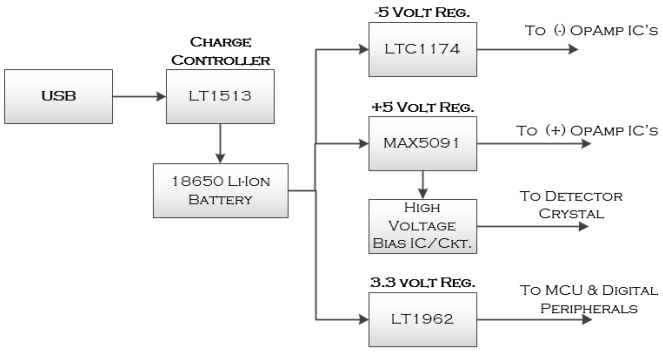


Fig. 10. Block diagram of power regulation.

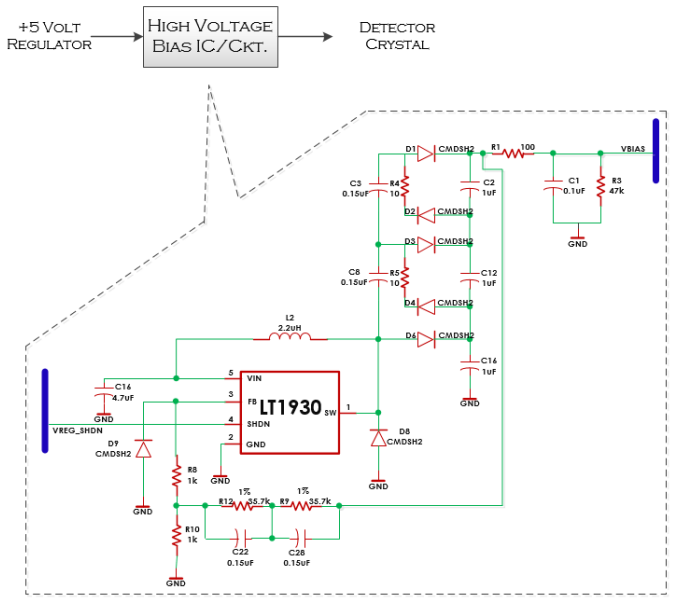


Fig. 11. High voltage bias supply implementation.

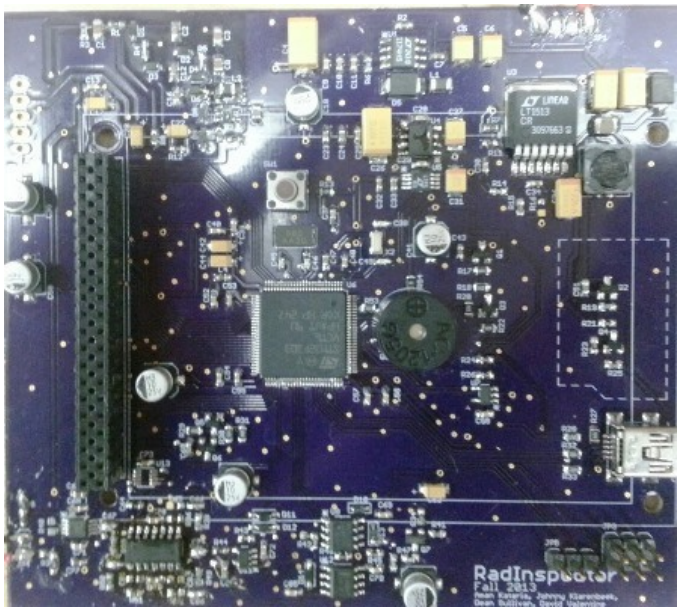


Fig. 12. RADInspector final PCB.

MAX 5091. The circuit designed in figure 11 depicts the boost converter module and an external voltage multiplier circuit. In this topology, 5 volts goes into the boost converter and gets stepped-up to 30 volt. From there it gets fed into a diode-capacitor multiplier where the voltage is tripled, resulting in 90 volts output.

Although high voltage biasing is highly desired, one of the major setbacks is dark current generation. Dark current is a statistical signal fluctuation that arises from thermal energy within the crystal lattice. And as weve seen from predictions and our tests, the dark current generated is directly proportional to the amount of bias voltage applied to the semiconductor crystal. Therefore it was essential to find methods of reducing dark current, one of those methods is cooling. The temperatures we would need to attain in order to reduce dark current ranged from -20 C to -80 C. To accomplish this, we proposed the use of a thermoelectric cooler, which is an electrical two-sided ceramic device that absorbs heat from one side, and pumps it out to the other side. It cycles this process constantly, resulting in a hot side where all the heat was transferred and a cold side where all the heat was taken away. Optimally, the cold sided plate would be where the detector crystals reside and a heatsink on the other, so that there is always a maximum temperature differential. We tested this using a high wattage TEC, which resulted in temperatures between -13 C and -20 C. This proved very effective in terms of current noise reduction but ineffective due to condensation and inefficient power consumption. As a better alternative, we will be using dry ice. Dry ice, also known as solid carbon dioxide, will be used since it is inexpensive, condensation free, and allows for a much lower temperature of -80 C.

## VII. Conclusion

The design and prototype of the RadInspector was mostly successful, however, as expected some minor changes were necessary from the conceived idea to the end product. Figure 12 shows our PCB design. Initially, we chose to implement a silicon detector, but finally chose the CZT (Cadmium Zinc Telluride) compound semiconductor for the detector, due to low cost and an overall improved spectrum. Consequently, this led to altering a few design aspects from our original design document. Another challenging part of this project was filtering out noise to ensure that an accurate spectrum was displayed. Digital signal processing was applied over analog processing in order to achieve a better SNR. To improve the RadInspector we would further experiment with different semiconductor detectors, invest in reliable test sources, optimize digital filtering techniques and implement a thermoelectric cooler to reduce noise. The engineering design aspects of this project were intriguing yet challenging, this kept us motivated to strive for excellence. Each group member was challenged with something new and has gained valuable experience in several areas.

Moreover, we were able to achieve the major design specifications such as; low power consumption, long battery life, room temperature operation for sources Americium-241 and Cesium-127 spectra, plot a spectrum and perform real-time dosimetry all under $500. We believe with more investment and research the device can be optimized.

## VIII. Acknowledgments

Throughout the course of the semester, our group had help from professors to professionals. Without their help, this project would not have moved along as smoothly as it did. First and foremost, we thank Dr. Samuel Richie for all of his guidance during the project design. Additional thanks to Dr. Elena Flitsiyan, Dr. Wasfy Mikhael, and Dr. Chung Yong Chan.

## IX. Biographies

Fig. 13. Dean Sullivan is a senior Electrical Engineering student at the University of Central Florida and will be graduating in December 2013. In Fall 2014, Dean will be attending graduate school for Electrical Engineering at UCF as an RA for Dr. Yier Jin.

Fig. 14. Aman Kataria is a senior Electrical Engineering student at the University of Central Florida and will be graduating in December 2013. Upon graduation, Aman will be attending graduate school for Biomedical Engineering.

Fig. 15. Johnny Klarenbeek is a senior Electrical Engineering student at the University of Central Florida and will be graduating in December 2013. Upon graduation, Johnny will work for Texas Instrument as a Design Verification Engineer.

Fig. 16. David Valentine is a senior Electrical Engineering student at the University of Central Florida and will be graduating in December 2013. Upon graduation, David will work for Lockheed Martin as a Systems Integration Test Engineer.